Regional 3-D Geophysical Characterization of the Nevada National Security Site

Leiph Preston[1], Christian Poppeliers[1], and David Schodt[1,2]

1. Geophysics Department, Sandia National Laboratories, Albuquerque, NM
2. Now at University of New Mexico, Albuquerque, NM

Abstract

We perform a joint inversion of absolute and differential P and S body waves, gravity measurements, and surface wave dispersion curves for the 3-D P- and S-wave velocity structure of the Nevada National Security Site (NNSS) and vicinity. Data from earthquakes, past nuclear tests, and other active source chemical explosive experiments, such as the Source Physics Experiments (SPE), are combined with surface wave phase and group speed measurements from ambient noise, source interferometry, and active source experiments to construct a 3-D velocity model of the site with resolvable structures as fine as 6 km horizontal and 2 km vertically. Results compare favorably with previous studies and expand and extend the knowledge of the 3-D structure of the region. More detailed information is provided in Preston et al. (2019, in prep).

Introduction

One of the goals of the Source Physics Experiments (SPE) is to gain a better understanding of the generation and evolution of seismic wave types over a range of propagation distances. Fundamentally, this requires accurate 3-D earth structural models of the site. We have developed a 3-D local-to-regional scale seismic velocity model of the NNSS using a joint inversion of body wave travel times, gravity measurements, and surface wave dispersion curves. Joint inversion of these disparate data types in a single unified model can enhance model accuracy by allowing the weaknesses of one data type to be mitigated by the addition of another data type (e.g., Syracuse et al., 2017). For example, body waves tend to have poor resolution in the shallowest portion of the crust since they are traveling nearly vertically there, but they can have good resolution at seismogneic depths. Gravity measurements, on the other hand, display a well-known trade-off between depth and anomaly size. By combining body wave and gravity information, both the shallow and deeper portions of the model can be resolved. Similarly, surface waves have frequency dependent depth sensitivity, again, allowing both shallow and deeper structures to be better resolved when combined with body wave data.

The NNSS is situated in the southern Walker Lane Belt (Stewart, 1988) in the broader context of the Basin and Range province. The NNSS in particular displays many of the general features of these geological regions, but in particular, is punctuated by volcanic and igneous rocks primarily from Miocene and later volcanic activity, including several overlapping calderas on the western side of the NNSS (e.g., O'Leary et al., 2002). As such, most of the local basins and mesas are at least partially covered or filled with volcanic tuffs. Yucca Flat, the locale of the SPE and DAG (Dry Alluvium Geology) experiments, is an alluvium and tuff filled basin surrounded by ranges surficially covered by silicic volcanics with exposures of pre-Cenozoic rocks (Phelps et al., 1999).

Data

We combine P- and S-wave travel times from body waves, differential P- and S-wave times from cross-correlation of earthquake records, gravity data, and surface wave group and phase speed dispersion curves into a single unified model of 3-D P- and S-wave wave speeds of the NNSS. P- and S-wave absolute and differential travel times for local earthquakes from 2000-2014 are

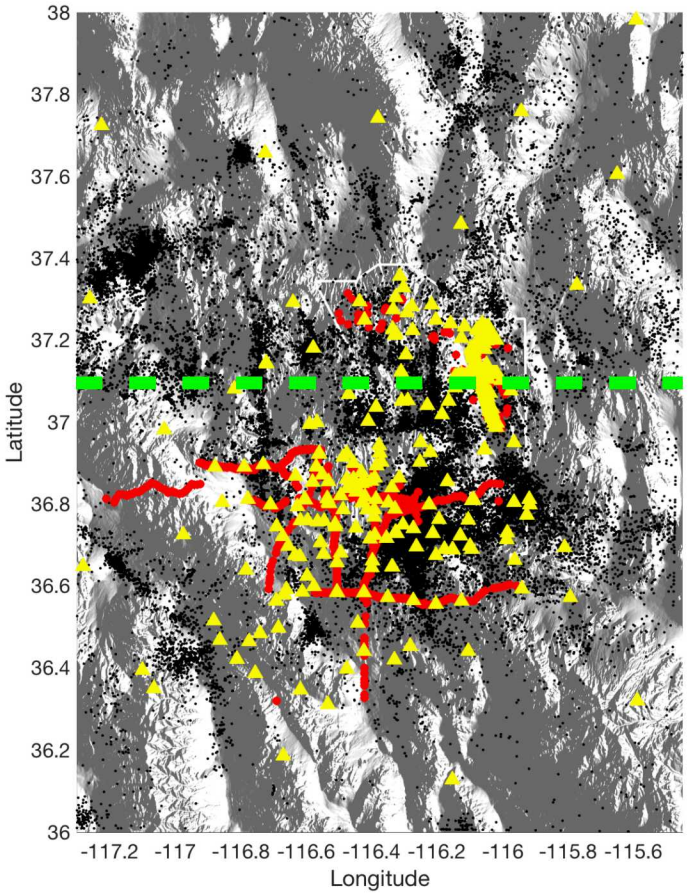

Figure 1: Overview map of the body-wave dataset. Shown are seismic stations (yellow triangles), active sources (red circles), and earthquakes (black dots). Green dashed line indicates the location of cross-section images.

derived from the UNR southern Nevada network catalog. P- and S-differential picks are based on cross-correlations of local earthquake waveforms from the UNR catalog. Data from active sources include arrivals from experiments performed around and near Yucca Mountain by the USGS in the 1980's and from nuclear tests conducted from 1980-1992 collected on the USGS on-site network. Also included are P-wave travel times from the SPE Large-N array (Mellors et al., 2018), P-wave arrival times and surface wave dispersion curves from the THOR1 and THOR2 experiments (Toney et al., submitted), absolute P-arrivals from the NPE (Denny, 1994), Watusi experiment (Bhattacharyya et al., 2003), and from SPE itself. Gravity data was harvested from the University of Texas El Paso's gravity and magnetic data repository (**http://research.utep.edu/Default.aspx?tabid=37229**). Our team picked dispersion curves from cross-correlation of ambient noise from UNR stations, processed using the MSNoise software package (Lecocq et al., 2014), and from source interferometry of the SPE and large-N arrays.

The study region extends from 36°-38° N latitude and from 115.5°-117.3° W longitude (about 220 km N-S by 160 km E-W) centered on the NNSS (Figure 1) and from the surface down to ~40 km depth. The dataset includes 535 unique seismic stations, 9,084 active source events, and

66,815 local earthquakes in addition to gravity observations. Table 1 gives the number of observations of each data type. Figures 2-4 indicate the distribution of UNR ambient noise

Table 1: Number of observations by data type

Data Type	Number
Abs P	738,830
Abs S	344,787
Diff P	297,144
Diff S	196,966
Gravity	24,723
Group	91,949
Phase	237

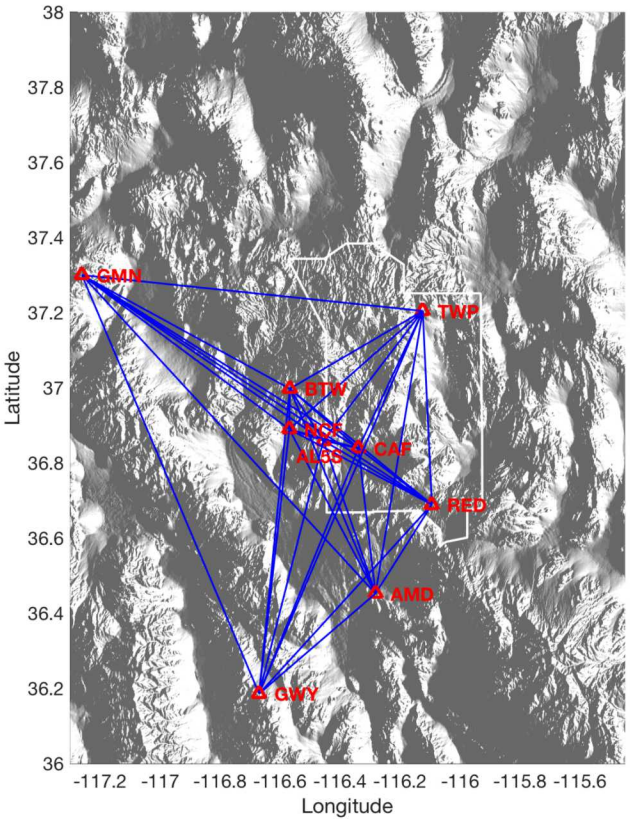

Figure 2: UNR stations used to derive surface wave dispersion from ambient noise

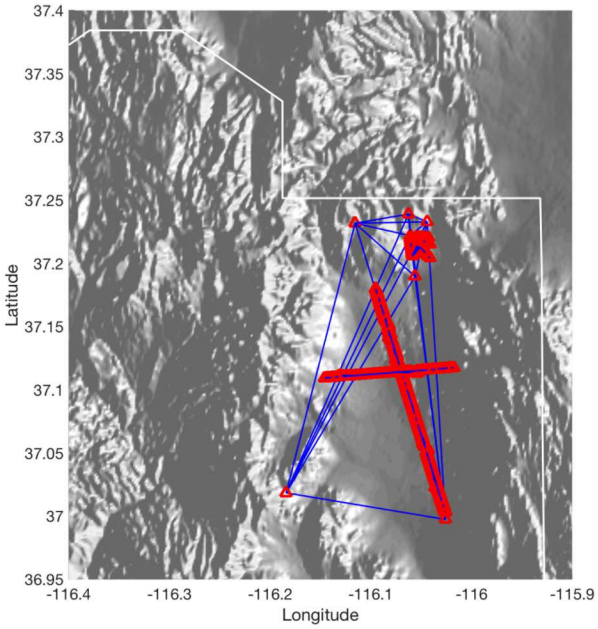

Figure 3: Northeast NNSS ambient noise, source interferometry, and active source surface wave dataset.

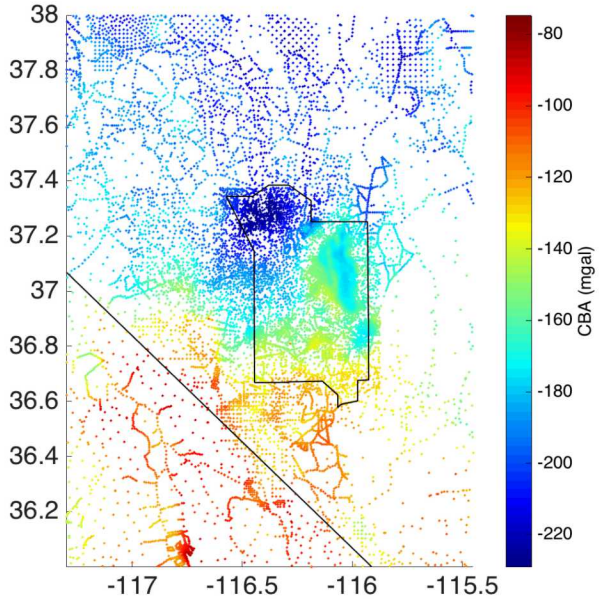

Figure 4: Gravity measurement points colored by complete Bouguer Anomalies

.

stations, Yucca Flat surface wave data, and gravity observations, respectively. The model region is discretized for tomographic inversion into 2x2x1 km blocks in x, y, z, respectively.

Method

The tomographic imaging process is a linearized, iterative inversion procedure that solves in a least squares sense for the optimal changes in the model given the current residuals. The entire system is regularized by constraining the P and S models to be smooth in a Laplacian sense. We utilize a bound version of Conjugate Gradient Least Squares (CGLS) to solve the regularized system of equations.

P and S body waves utilize the Vidale-Hole finite-different eikonal solver (Hole and Zelt, 1995; Vidale, 1990) to find the 3-D ray paths, travel times, and resulting sensitivities through the current model. Active source seismic data have fixed and known locations in time and space. However, earthquakes do not; as such, earthquake hypocentral locations are also solved for during the inversion process. Additionally, the nuclear tests indicated timing discrepancies that were accounted for by allowing their origin times to drift during inversion.

Each gravity observation is dependent on the densities in the entire 3-D volume. The conversion between densities and P-wave velocities is achieved through an admixture of Brocher (2005) and Gardner's relation (Gardner et al., 1974) to include both higher and lower P-velocities. Sensitivities to changes in the P-wave model are based on the derivative of this density-Vp mathematical relation.

In map view, the surface wave sensitivity area is constructed using the frequency-dependent surface wave kernels of Lin and Ritzwoller (2010). This 2-D surface is then downward continued to create a 3-D sensitivity volume. The 3-D P- and S-wave nodes within this volume are then converted into a 1-D velocity model, which is used to solve for the Rayleigh wave phase and group speeds (Lysmer, 1970). The 1-D velocities layers are then each perturbed to find the model sensitivities via finite differences.

Results and Discussion

The tomographic inversion results in a 3-D Vp and Vs structural model of the NNSS and vicinity. Figures 5-11 show some example depth- and cross-sections for Vp and the Vp:Vs ratio with all depths being relative to mean sea level (MSL). In these figures, black dots are sources (relocated earthquakes, nuclear explosions, or active sources) draped over a shaded relief map. Colors indicate the velocity or Vp:Vs ratio only where body wave ray paths exist. However, gravity and surface wave data affect large volumes within the model; thus, even grey regions have been influenced to some degree by these data directly.

Checkerboard resolution tests are a means of assessing the ability of the inversion to resolve structures of various spatial scales given the distribution of data and data errors. These tests indicate that the highest resolution of 6 km horizontally and 2 km vertically for P-waves is located generally within the NNSS proper, from the surface down to about 5 km depth. Larger scale blocks (to 40 km) show resolution over nearly the entire model region (except the very northern and eastern portions), down to about 15 km depth, which coincides approximately with the maximum depth of seismicity in the region. Error analysis demonstrates that with data errors

adjacent structures with contrasts of about 10-15% are resolvable at all scales evaluated. S-wave resolution is roughly similar to the P-wave resolution, except that the minimum resolvable scale is 10 km horizontally and the horizontal coverage of high resolution is somewhat more restricted compared to P-waves. However, due to the presence of surface wave data, S-waves have better resolvability at depths greater than ~5 km.

The P-wave model shows strong correlation with surface topography, with high Vp mountain ranges and low Vp basins, primarily controlled by the gravity data. The -1 km depth section (Figure 5) is the shallowest layer of the model with a significant portion below the local topography. Yucca Flat shows a lower velocity eastern part of the basin compared to the west, with the transition roughly coincident with the Carpetbag Fault (Phelps et al., 1999), which was not resolvable until the addition of the THOR data set.

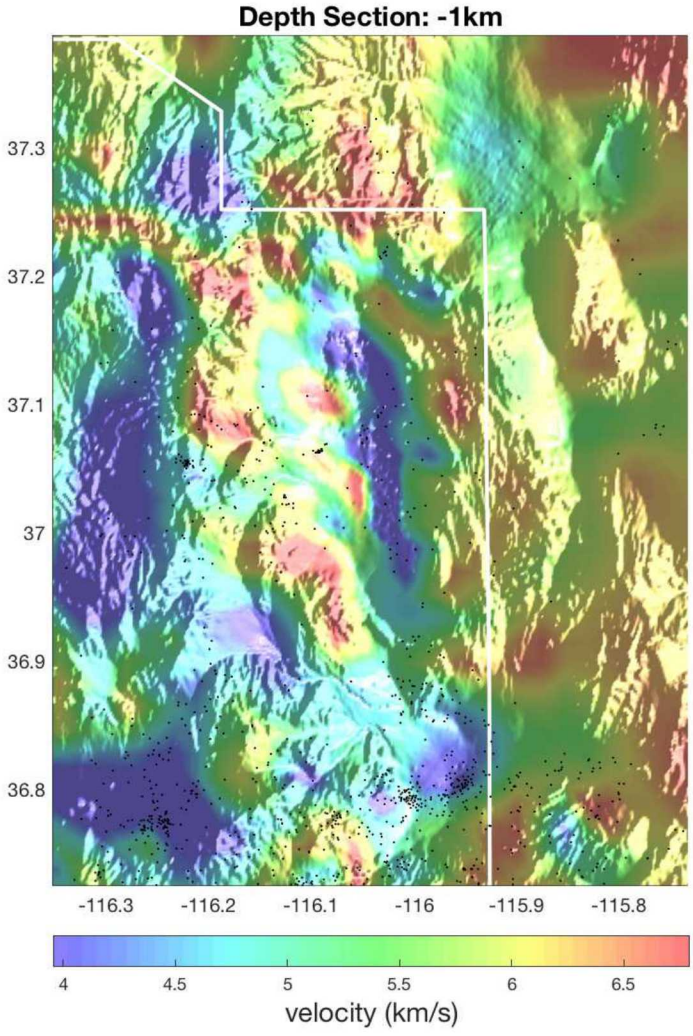

Figure 5: Vp depth-section at -1 km depth (re MSL, i.e., 1 km above MSL) focused on Yucca Flat.

At 0 km depth (Figure 6), all of the model region is below the topography except Death Valley. At this depth, we are generally below Yucca Flat's Cenozoic fill except at its southern end (Phelps et al., 1999). However, basins in the southern NNSS clearly are depicted by low Vp regions. Low Vp regions not associated with basins in the NNSS occur in Pahute Mesa and east of Timber Mountain. Vp/Vs (Figure 7) is generally at or above 1.73 throughout the NNSS, with a larger high Vp/Vs region running roughly north-south through the center of the NNSS.

For depths greater than 3 km (Figure 8), we are below the low-velocity basins. However, low velocities still exist within Pahute Mesa and a low velocity region has returned under Yucca Flat extending southward under Frenchman Flat. The checkerboard analysis indicates marginal resolution of a feature this size under Yucca Flat, but it is resolvable in the south, where it coincides with a cluster of earthquakes. The low Vp under Pahute Mesa is still evident at 6 km depth, whereas most of the NNSS is at or above average Vp except, again, the small region coincident with a cluster

of earthquakes under Frenchman Flat (Figure 9). Vp/Vs at 6 km depth (Figure 10) remains at or above 1.73 except under Pahute Mesa and under southern Yucca Flat.

East-west cross-sections of Vp about halfway through Yucca Flat (Figure 11) clearly show the shallow basin

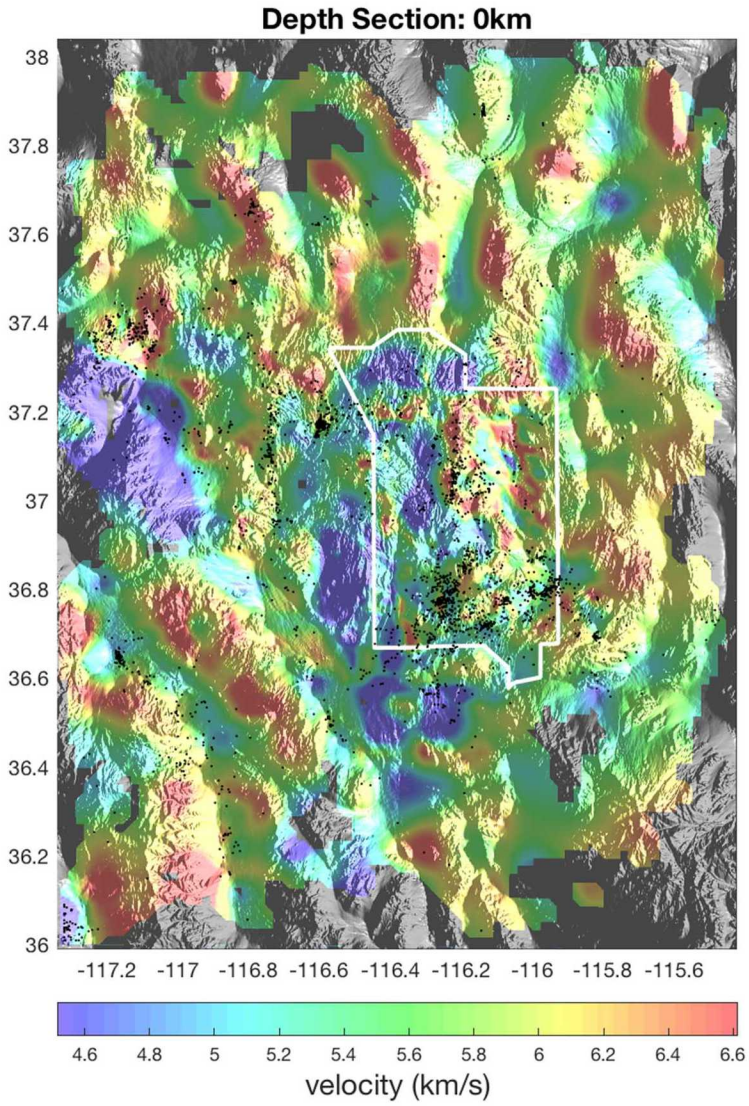

Figure 6: Vp depth-section at 0 km depth (MSL)

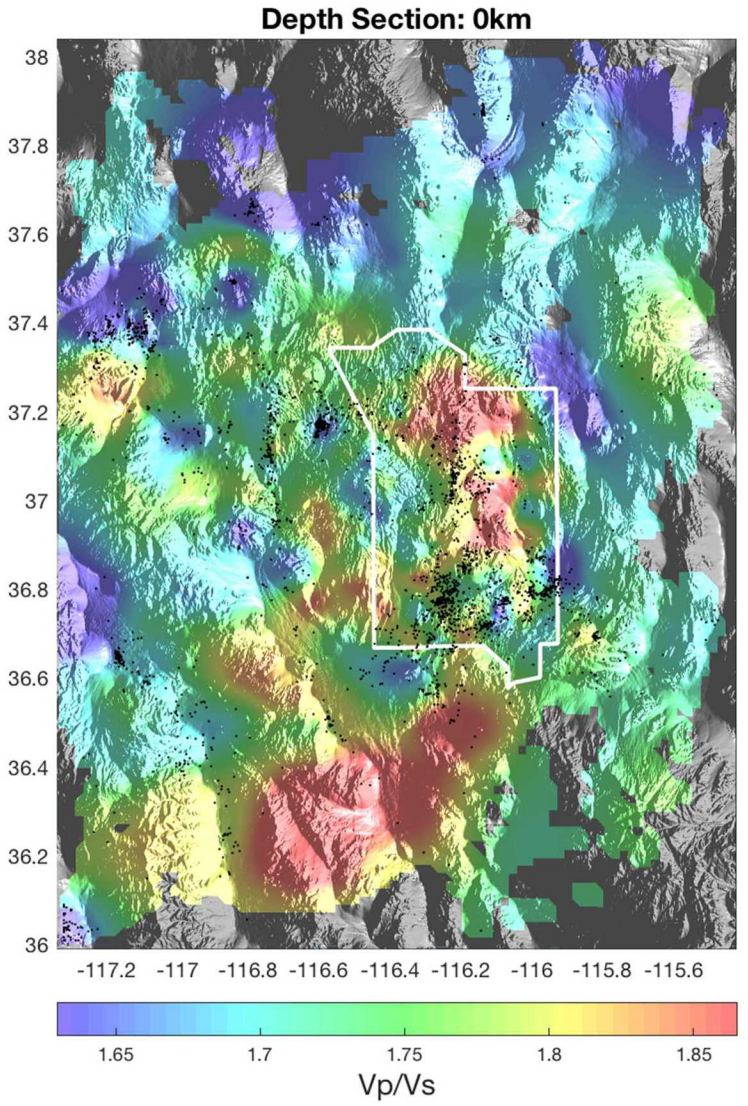

Figure 7: Vp/Vs depth-section at 0 km depth (MSL)

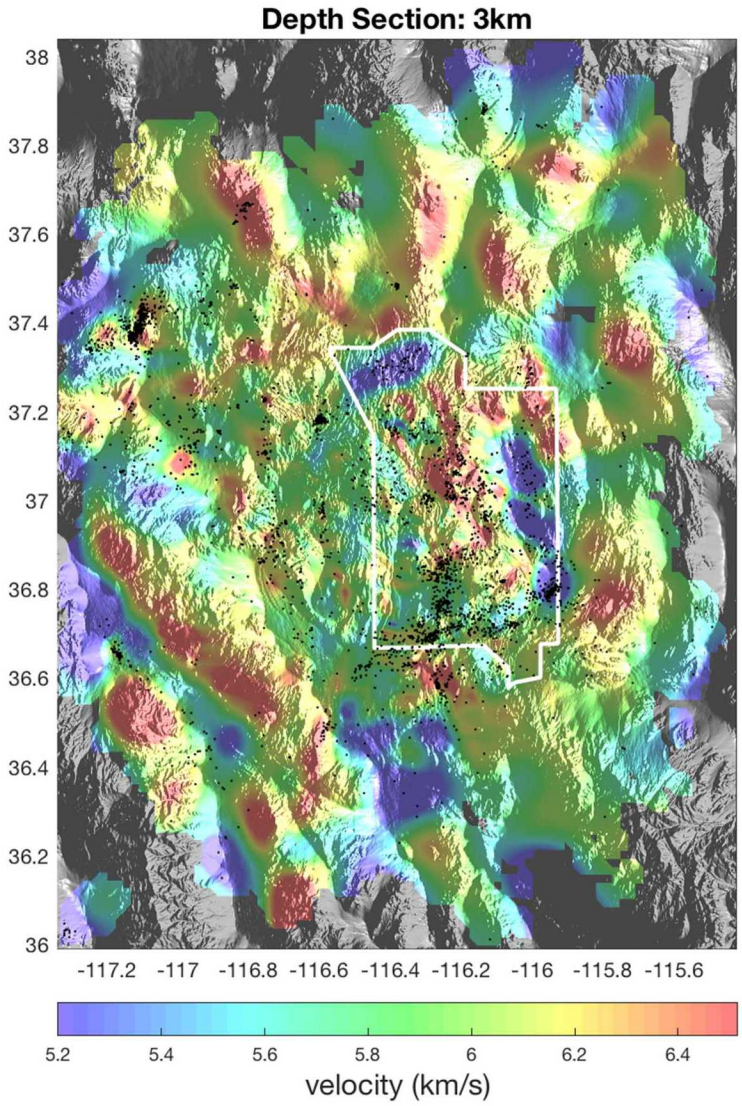

Figure 8: Vp depth-section at 3 km depth (re MSL)

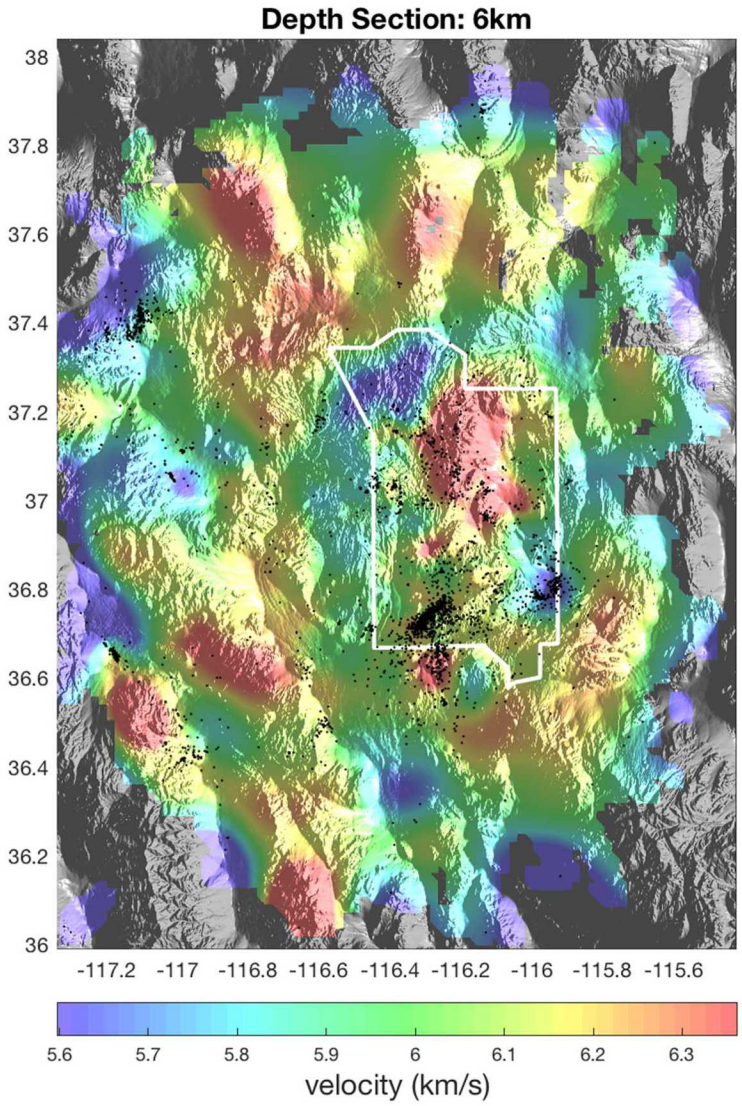

Figure 9: Vp depth-section at 6 km depth (re MSL)

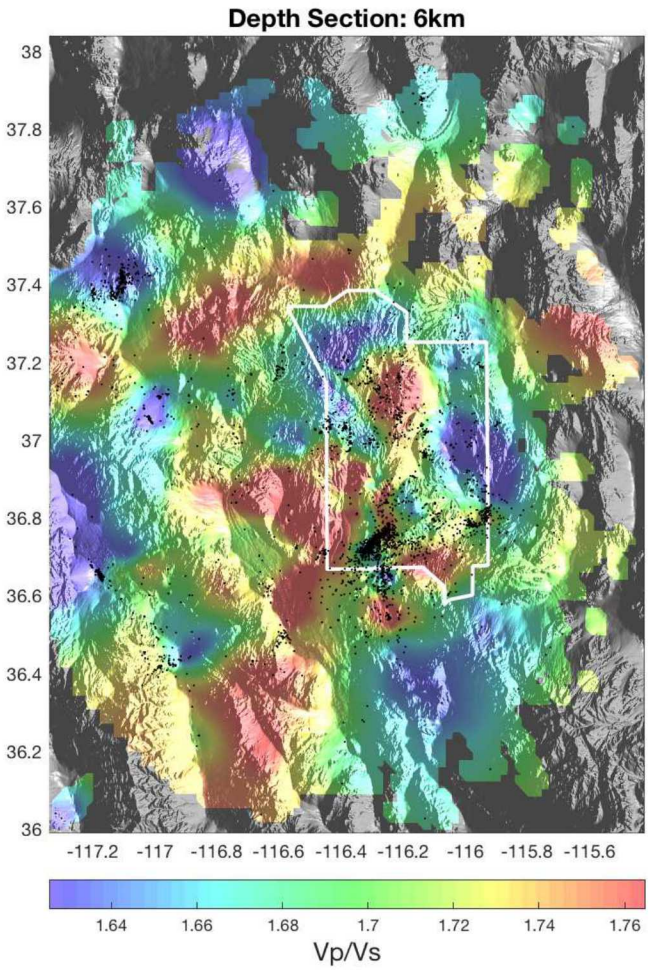

Figure 10: Vp/Vs depth-section at 6 km depth (re MSL)

structure of Yucca Flat with a shallower western portion compared to east. Also, Timber Mountain can be identified by the broad high velocity region that extends to the surface surrounded by lower velocity regions both to the west and east. Vp/Vs (not shown) averages near 1.75 at the surface except under Yucca Flat and to its west, where higher than average Vp/Vs ratios predominate. Please see Preston et al. (in prep) for more detailed analysis.

Conclusions

We have produced a 3-D Vp and Vs seismic velocity model of the NNSS and vicinity using a joint inversion of absolute and differential body wave arrival times, gravity observations, and measurements of surface wave dispersion. Joint inversion using these disparate data types enhanced overall model resolvability by allowing the weaknesses in one data set to be mitigated by the strengths of another. The highest resolution is achieved within NNSS proper to about 5 km depth. The 3-D model resolves many known structures in the region, making it well-suited for regional full waveform modeling, but also indicates regions that may be of interest for future studies.

Acknowledgements

The authors wish to thank David von Seggern for providing the cross-correlation differential body wave travel times, Rob Abbott for the body and surface wave data from the THOR experiments, Ting Chen for the Large-N P-wave arrival times, Tom Brocher for the USGS Yucca Mountain active source data, and Chrysm Watson-Ross for installation and processing for the MSNoise software.

Sandia National Laboratories is a multimission laboratory managed and operated by National Technology & Engineering Solutions of Sandia, LLC, a wholly owned subsidiary of Honeywell International Inc., for the U.S. Department of Energy's National Nuclear Security Administration under contract DE-NA0003525.

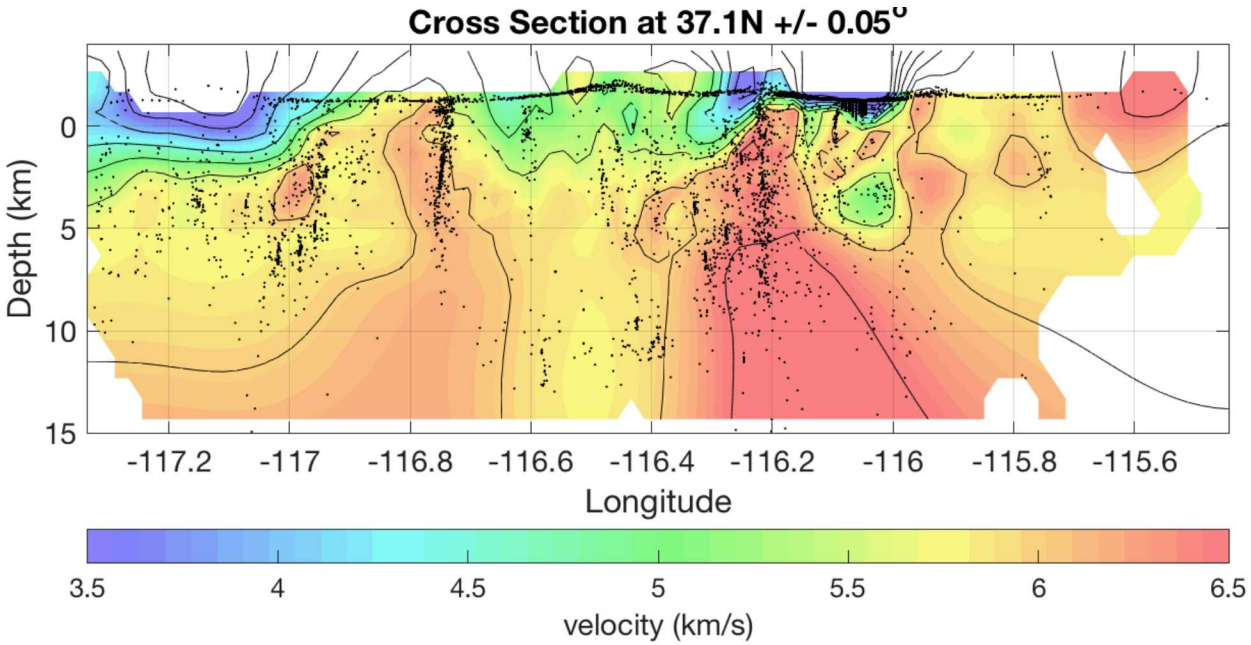

Figure 11: Vp cross-section at 37.1°N (dashed line in Figure 1).

This paper describes objective technical results and analysis. Any subjective views or opinions that might be expressed in the paper do not necessarily represent the views of the U.S. Department of Energy or the United States Government.

References

Bhattacharyya, J., H.E. Bass, D.P. Drob, R.W. Whitaker, D.O. Revelle, and T.D. Sandoval, Description and analysis of infrasound and seismic signals recorded from the Watusi explosive experiment, September 28, 2002, in *Proceedings of the 25th Seismic Research Review - Nuclear Explosion Monitoring: Building the Knowledge Base*, Tucson, Arizona, LA-UR-03-6029: Vol. 2, pp. 587-596, 2002.

Brocher, T.M., Empirical relations between elastic wavespeeds and density in the earth's crust, *Bull. Seis. Soc. Am.*, 95 (6), 2081-2092, doi: 10.1785/0120050077, 2005.

Denny, M.D. (Editor), *Proc. of the Symposium on the Non-Proliferation Experiment (NPE): Results and Implications for the Test Ban Treaties*, 19-21 April 1994, Rockville, Maryland, CONF 9404100, Lawrence Livermore National Laboratory, 1994.

Gardner, G.H.F., L.W. Gardner, and A.R. Gregory. Formation velocity and density—the diagnostic basics for stratigraphic traps, *Geophysics* 39, 770–780, 1974.

Hole, J. and B. Zelt, 3-D finite-difference reflection traveltimes, *Geophys. J. Int.*, 121(2), 427-434, 1995.

Lin, F-C. and M.H. Ritzwoller, Empirically determined finite frequency sensitivity kernels for surface waves, *Geophys. J. Int.*, doi: 10.1111/j.1365-246X.2010.04643.x, 2010.

Lecocq, T., C. Caudron, and F. Brenguier, MSNoise, a Python Package for Monitoring Seismic Velocity Changes Using ambient seismic noise, *Seis, Res. Lett.*, 85(3), 715-726, 10.1785/0220130073, 2014.

Lysmer, J., Lumped mass method for Rayleigh waves: *Bull. Seis. Soc. Am.*, 60, 89–104, 1970.

Mellors, R.J., A. Pitarka, E. Matzel, S. Magana-Zook, D. Knapp, W.R. Walter, T. Chen, C.M. Snelson, and R.E. Abbott, The Source Physics Experiments Large N Array, Seis. Res. Lett., 89(5), 1618-1628, 10.1785/0220180072, 2018.

O'Leary, H.W., D. W., E. A. Mankinen, R. J. Blakely, V. E. Langenheim, and D. A. Ponce, Aeromagnetic expressions of buried basaltic volcanoes near Yucca Mountain, Nevada, *U.S. Geol. Surv. Open File, 02 – 020*, 2002.

Phelps, G.A., V.E. Langenheim, and R.C. Jachens, Thickness of Cenozoic deposits of Yucca Flat inferred from gravity data, Nevada Test Site, Nevada, *U.S. Geol. Surv. Open File, 99-310*, 1999.

Preston, L., C. Poppeliers, and D. Schodt, Seismic Characterization of the Nevada National Security Site Using Joint Body Wave, Surface Wave and Gravity Inversion, in submission to *Bull. Seis. Soc, Am.*

Stewart, J.H., Tectonics of the Walker Lane Belt, western Great Basin; Mesozoic and Cenozoic deformation in a zone of shear, in *Metamorphism and Crustal Evolution of the Western United States*, ed. W.G. Ernst, 683-713, Prentice-Hall, Englewood Cliffs, NJ, 1988.

Syracuse, E.M., H. Zhang, and M. Maceira, Joint inversion of seismic and gravity data for imaging seismic velocity structure of the crust and upper mantle beneath Utah, United States, *Tectonophysics*, **718**, 105-117, 10.1016/j.tecto.2017.07.005, 2017.

Toney, L.D., R.E. Abbott, L.A. Preston, D.G. Tang, T. Finley-Hatton, and K.E. Phillips-Alonge, Joint body- and surface-wave tomography of Yucca Flat, NV using a novel seismic source, in submission to *Bull. Seis. Soc. Am.*

Vidale, J., Finite-difference calculation of traveltimes in three dimensions, *Geophysics*, 55(5), 521-526, 1990.